Synergistic activity of silver nanoparticles and polyamino-cyclodextrins in nanosponge architectures

Marco Russo,[a] Alberto Spinella,[b] Antonella Di Vincenzo,[a] Giuseppe Lazzara,[c] M. Rita Correro,[d] Patrick Shahgaldian,[d] Paolo Lo Meo*[a] and Eugenio Caponetti[a,b]

Abstract: Four new composite materials, formed by silver nanoparticles embedded in polyamino-cyclodextrin nanosponge architectures, were designed exploiting the affinity of polyamino-cyclodextrins towards Ag^+ ions. These materials were characterized by means of different techniques (thermogravimetry, FT-IR, solid state NMR, SEM, HR-TEM), and tested as catalysts for the reduction of nitroarenes and the oxidative coupling of anilines. The results obtained showed synergistic activity between the supramolecular binding abilities of the nanosponge matrix and the catalytic properties of the metal nanoparticle, and open the way towards the design of new composite smart nanomaterials with improved catalytic performances.

Introduction

Noble metal nanoparticles (**NP**s) display valuable catalytic properties, due to their peculiar surface-to-volume ratio and electronic features. However, their manipulation is often challenging, and immobilization on inert supporting materials or polymeric matrices[1] is required, in order to implement large-scale sustainable chemical processes.[2] Therefore, coupling with supramolecular host systems able to capture the transforming substrate, might result in a rewarding strategy to achieve enhanced activity.[3] Nanosponges (**NS**s),[4] which are hyper-reticulated polymers made of host units joined by means of suitable linker units, constitute an interesting potential platform for building new NP-based systems with improved performances. In particular, cyclodextrin-based nanosponges (**CDNS**s) represent the most studied class of NSs, taking advantage from the chemical versatility and easy availability of the host monomer. Indeed, cyclodextrins (**CD**s) can include and transport structurally diverse organic species[5], and the thermodynamic and microscopic aspects of their binding equilibria have been thoroughly investigated.[6] In addition, the structure of CDs allows a variety of chemical transformations.[7] The properties of CDNSs (pore size, thermal stability, responsivity to external stimuli, adsorption or controlled release abilities towards organic guests) can be largely tuned up by a suitable choice of the linker unit.[8] The possibility to jointly exploit the peculiar features NSs and NPs has started to attract the interest of researchers only recently, and relevant up-to-date literature is scarce. In particular, Li[9] and Vasconcelos[10] have used different CDNSs to support Au NPs as catalysts for the reduction of *p*-nitrophenol, whereas hybrid inorganic-organic materials containing CDNSs and Pd NPs have been designed by Sadjadi for C-C bond formation reactions.[11] CD oligomers have been used to stabilize Au NPs[12] or Ru NPs.[13] Synthetic strategies may provide either the inclusion of pre-formed NPs in the NS or the reduction in situ of the metal cation; in the latter case, the organic material may occasionally function also as the reductant.

Some of us have recently described[14] the synthesis and pH tunable adsorption abilities of four new CDNSs (**ANS1-ANS4**, Scheme 1), bearing different polyamines (**A1**-**A4**) as the linker units (relevant analytical data are collected in the Supporting Information, Table S1). We incidentally observed that these materials are able to sequestrate Ag^+ ions with high efficiency from aqueous solution, consistent with the well-known affinity of Ag^+ towards N-donor ligands. The free polyamino-CDs[15] (**ACD**s) are known to form large aggregates in solution with Ag^+, easily affording NPs capped with several layers of ACD units upon treatment with formaldehyde or $NaBH_4$[16] or even by light irradiation.[17] Despite the widespread applications that Ag NPs have found in several fields, spanning from catalysis[18] to theranostics[19] and antibacterial agents[20], the possibility to support them into NS architectures has not been explored yet. Hence, the present work is aimed at showing that, by exploiting the aforementioned sequestering abilities of materials **ANS1-ANS4** towards Ag^+, it is possible to accomplish the preparation of four composites, constituted by Ag NPs embedded in the NS matrix (indicated hereinafter as **NAPS1-NAPS4**, Scheme 1), and that these materials possess an improved catalytic activity towards some typical probe reactions (namely, the reduction of nitrand the oxidative coupling of anilines).

Results and Discussion

Synthesis and characterization of the composites. The synthesis of materials **NAPS1**-**NAPS4** (see Experimental for details) provides that the pristine pre-formed polyamine-CDNSs are equilibrated with an excess of aqueous $AgNO_3$ to form four precursor materials (**P1**-**P4**), which are subsequently subjected to reduction with $NaBH_4$. The reaction can be easily followed by visual color changes. In fact, the pristine pale brown starting material turns brown-reddish after adsorption of Ag^+, and finally

[a] Dr. M. Russo, Dr. A. Di Vincenzo, Prof. E. Caponetti, Prof. P. LoMeo
Department STEBICEF
University of Palermo
V.le delle Scienze pad. 17 – 90128 Palermo (Italy)
E-mail: paolo.lomeo@unipa.it
[b] Dr. A. Spinella, Prof. E. Caponetti
Centro Grandi Apparecchiature - ATeNCenter
University of Palermo
Via F. Marini, 14 – 90128 Palermo (Italy)
[c] Prof. G. Lazzara
Department of Physics and Chemistry
University of Palermo
V.le delle Scienze pad. 17 – 90128 Palermo (Italy)
[d] Dr. M. R. Correro, Prof. P. Shahgaldian
Institut für Chemie und Bioanalytik
Hochschule für Life Sciences FHNW
Hofackerstrasse 30 - 4132 Muttenz (Switzerland)

Supporting information for this article is given via a link at the end of the document.

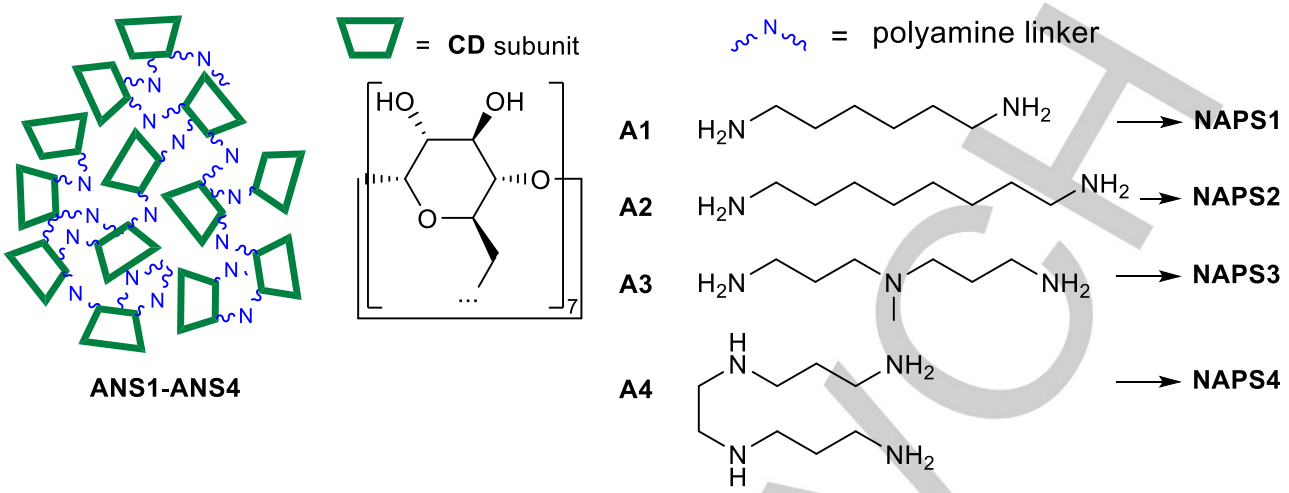

Scheme 1. Structures of polyamine-**CDNS**s.

black upon treatment with $NaBH_4$. The composites were repeatedly washed (with water, methanol and diethyl ether) and ultimately dried in vacuo. It is worth noting that the final materials may lose part of the NP content during workup, as accounted for by the typical reddish color assumed by the aqueous liquors. So, water washing was iterated until the liquors were colorless.

Precursors **P1**-**P4** and final materials **NAPS1**-**NAPS4** were first characterized by thermogravimetric analysis (TGA) in order to determine their silver loading. Thermogravimetry is a technique of choice to assess the composition of complex or hybrid materials,[11a] which has been already successfully applied composites containing Ag nanoparticles.[21] The TGA curves for **NAPS2** and its precursors **ANS2** and **P2** are shown in Figure 1 as representative examples (see complete data in the Supporting, Table S2). From the percent weight of Ag, the mole ratio between the metal and the N donor atoms in the matrix can be easily calculated. For precursors **P1**-**P4**, data surprisingly indicate that the largest amount of Ag^+ (27.2 % in weight) is present in the material with the most hydrophobic linker **A2**. Probably, the hydrophobic character of the linker favors the formation of aqueous clusters in the matrix, causing the retention of the largest amount of Ag salt. After reduction, the same material also showed the largest metal loss upon washing; Ag loss decreased on decreasing the hydrophobic character of the linker, and resulted negligible for **NAPS4**, having the most hydrophilic linker **A4**. Large metal loadings are observed (which range from 18.8 to 24.4 % in weight, in good agreement with values reported elsewhere[22]), due to the high affinity of the pristine NS towards Ag^+ and the relatively low porosity of the material, which hampers the loss of the formed particles.

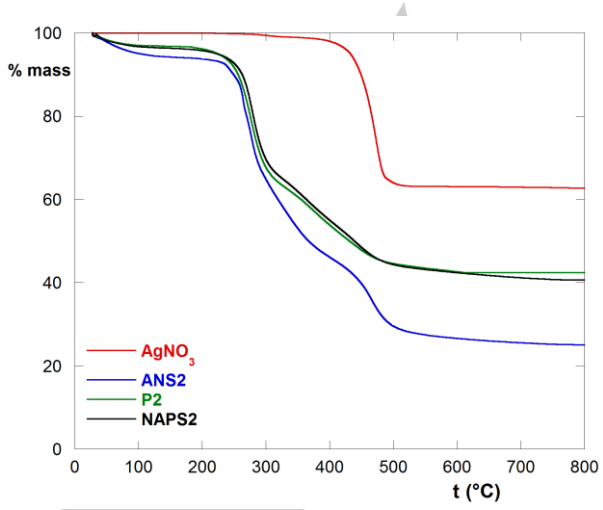

Figure 1. TGA curves of $AgNO_3$, **ANS2**, **P2** and **NAPS2**.

Spectroscopic characterization of the composites was performed by FT-IR and solid-state NMR (spectra of **ANS2**, **P2** and **NAPS2** are shown as representative examples). In the FT-IR spectra (Figure 2) the signals cluster typical fingerprint of the CD scaffold can be noticed at 1200~1000 cm^{-1}, which does not undergo any significant modification for the three materials. This indicates that neither the absorption of Ag^+ nor the subsequent reduction affect the overall stability of the CDNS matrix. Rather, it is interesting to notice the fate of the tiny N-H bending band at 750 cm^{-1} of pristine **ANS2**. This signal decreases in intensity for **P2**, while a new band appears at 824 cm^{-1} due to the N···Ag^+ interaction. Subsequent reduction causes the decrease in intensity of the latter signal with respect to the one at 750 cm^{-1}. Similar bands have been also observed for the soluble Ag/ACD nanocomposites mentioned previously.[16] Another remarkable set of bands can be identified in the low frequency region (130~30 cm^{-1}), where the ligand-metal vibration modes signals occur. Pristine **ANS2** shows two bands at 37.6 and 55.7 cm^{-1}, present also in the subsequent composites. On the other hand, **P2** shows further peaks at 42.0 and 46.9 cm^{-1}, whereas **NAPS2** shows new peaks at 45.8, 52.2 and 71.6 cm^{-1}. All the latter bands can be attributed to Ag···N vibrations.[23]

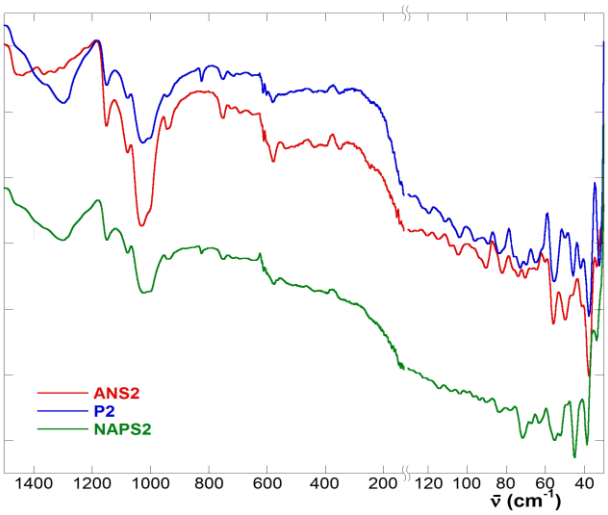

Figure 2. FTIR spectra of **ANS2**, **P2** and **NAPS2**.

Solid state $^{13}C\{^{1}H\}$ CP-MAS NMR spectra (Figure 3) provided further confirmation of the Ag-CDNS interactions. The spectrum of **ANS2** shows five main signals at 29 ppm (methylene C of the linker chains), 51 ppm (methylene C of the linker chains bound to the N bridgehead atoms, overlapped with the C6 of the CD units), 73 ppm (CD C2, C3 and C5), 84 ppm (CD C4) and 103 ppm (CD C1). After absorption of Ag^{+}, the signal at 51 ppm undergoes a significant broadening and modification in shape, due to the N···Ag^{+} interactions, but recovers its original shape after reduction. These variations perfectly mirror the changes of the N-H bending bands in the FT-IR spectrum.

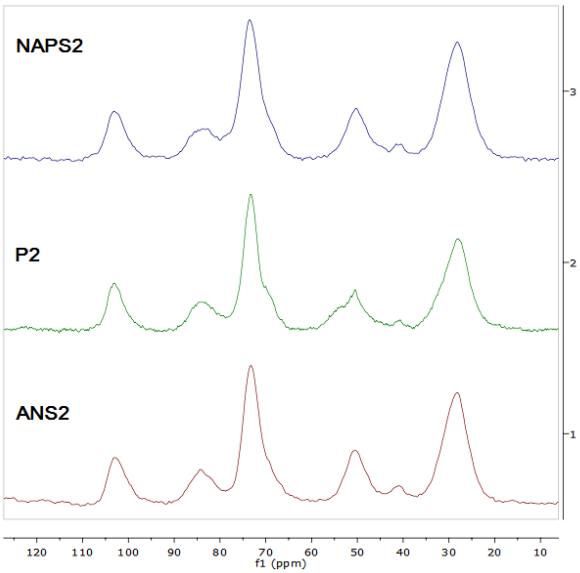

Figure 3. $^{13}C\{^{1}H\}$ CP-MAS spectra of **ANS2**, **P2** and **NAPS2**.

Morphological characterization of the final composites was performed by means of SEM and HR-TEM techniques (the complete collection of micrographs is given in the Supporting Information). From SEM micrographs (Figure 4). it can be noted that the grains of the material show a quite compact structure, although roughness and cavities can be evidenced on increasing the magnification level. On the grain surface small and well contrasted objects can be also observed, which may be identified as Ag NPs by comparison with TEM images. The latter technique provided complementary information (Figure 5). TEM micrographs reveal that the nature of the polyamine linker heavily affects the features of the composite. For **NAPS1** and **NAPS2**, with the most hydrophobic linkers, small and relatively polydispersed NPs are observed, showing an average diameter

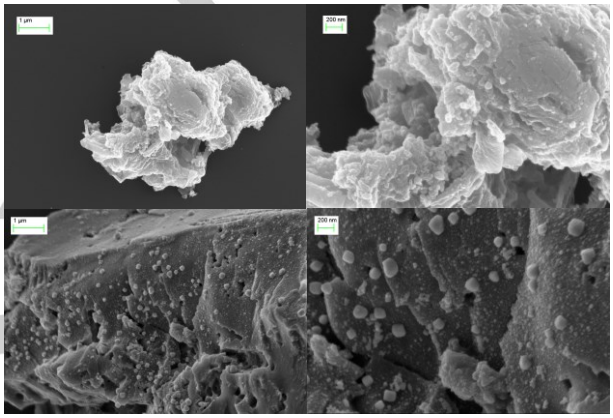

Figure 4 Selected SEM micrographs of materials **NAPS1** (top) and **NAPS4** (bottom).

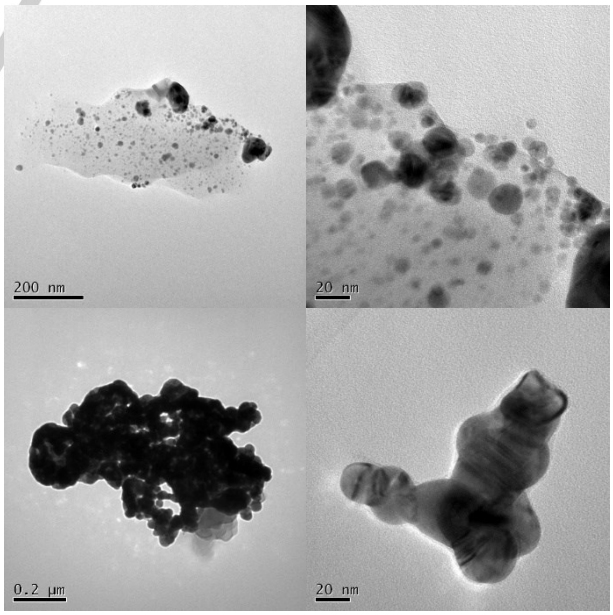

Figure 5. Selected TEM micrographs of materials **NAPS1** (top) and **NAPS3** (bottom).

of ca. 9.5 nm (which is significantly smaller than the one found for AgNPs capped by free ACDs[16]). The NPs appear quite well distributed within the organic matrix, although fair accumulation near the grain surface is apparent. By contrast, the materials with the most hydrophilic polyamine linkers **NAPS3** and **NAPS4**, show larger NPs; however, extensive coalescence occurs, hampering a reliable evaluation of the particle size and their statistical distribution; in addition, scattering effects make it difficult to distinguish grain edges.

Everything considered, all the evidences collected can be rationalized assuming that, after absorption of the Ag+ ion, the hyper-reticulated structure of the ANS functions as a sort of template providing a micro-environment for both the formation and the stabilization of the nanoparticles upon reduction with $NaBH_4$. This situation is significantly different from the one occurring in the formation of the ACD-capped Ag NPs in solution described in our previous works. In the latter case, indeed, Ag NP formation occurs from large ACD-Ag+ self-assembled aggregates, and the metal NP cores appeared stabilized onion-like by multiple layers of free ACD units held together by supramolecular interactions. Noticeably, these ACD layers are quite labile (as accounted for by both spectroscopic and kinetic evidences), so that the metal core surface may be left partly uncovered upon dilution; by contrast, for our NAPS systems the micro-environment provided to the metal NPs by the ANS supporting materials appears perfectly stable.

Catalysis tests. Materials **NAPS1-NAPS4** were tested as catalysts for two test reactions, namely the reduction of nitroarenes with $NaBH_4$ and the oxidative coupling of anilines. The former one in particular constitutes a standard for assessing the activity of NP-based catalysts. We used *p*-nitroaniline (**1**) and *N*-(*p*-nitrophenyl)-L-prolinol (**2**, Scheme 2) as model substrates, under conditions comparable with those reported for the homogeneous catalysis with aqueous free ACD-capped Ag NPs (40 °C, Ag 50 μmol/L).[16] The reaction was followed by monitoring the substrate absorbance at the proper λ_{max} (i.e. 378 nm for **1**, 420 nm for **2**) although the heterogeneous conditions did not allow performing true kinetic experiments. All composites showed a satisfactory efficiency: complete conversion was achieved in shorter times (2.5 min for **1**, 4 min for **2**) than observed by us[16] in the presence of free ACD-capped Ag NPs in solution (5 min for **1**, 7.5 min for **2**); the catalyst could be recovered and reused with no apparent loss of activity for at least 10 cycles. These results indicate a significant improvement of the catalytic performance due to the association of the Ag NPs with the NS, with no notable differences among the four materials.

The larger reactivity of **1** with respect to its *N,N-bis*-substituted derivative **2** deserves some consideration. In fact, for the reaction under homogeneous conditions the relative reactivity observed depends on the amount of ACD present in the system, due to both the stability of the ACD·substrate complex and the coverage of the NP surface, according to a complex multiple equilibria scheme.[16] Moreover, *N*-substituted *p*-nitroanilines show lower affinity for ANSs than the parent **1**, due to steric effects,[14] whereas the opposite occurs for free β-CD in solution. So, in order to clarify the role exerted by the nanosponge architecture in the reaction course, we built a homemade flux reactor constituted by a thermostated glass tube containing 100 mg of material **NAPS2**. Then, suitable test samples were fluxed through the catalytic bed at such a rate to allow a contact time consistent with the reaction times reported above (namely, 1.2 mL/min for **1**, 0.75 mL/min for **2**). We observed that *p*-nitroaniline **1** is quantitatively sequestered by the material, and then can be completely recovered by elution with methanol. When **1** was introduced with $NaBH_4$, both the reaction liquor and the subsequent methanol eluate showed no absorbance at 378 nm, indicating complete conversion of the starting nitroarene. By contrast, for the substituted substrate **2** the aqueous reaction liquor appeared colored in pale pink, and a 25% amount of unreacted nitroarene was recovered after methanol elution. The UV-vis spectrum of the pink solution, which shows three peaks at 476, 508 and 551 nm (see spectrum in Supporting), is consistent with the presence of traces of a *bis*-4,4'-(dialkylamino)-azobenzene derivative.[24] Such a by-product may be the result of the formation of a nitrosoarene intermediate,[25] which then reacts with the aniline product (Scheme 2). All these evidences allow drawing the following mechanistic hypothesis. The CDNS first captures the substrate, concentrating it close to the Ag NPs. According to literature, the polarized nitroarene points its nitro group towards the primary host rim on inclusion into the CD units.[26] Hence, we may speculate that the included nitroarene slips down through the CD primary rim to approach the **NP** surface and undergo the reduction reaction. Therefore, reactivity is disfavored by any possible steric effect due to the substitution on the amine N atom. This explanation is consistent with the results observed for the ACD-capped Ag NPs.[16] After the reduction has occurred, the product possesses a low affinity for the CD units due to its poor polarization, and is eluted away from the NS. Reduction of the nitro group likely occurs stepwise through a nitroso intermediate;[25] so, if the substrate reactivity the is relatively low, the intermediate might accumulate and react with the final aniline to afford the azobenzene by-product.

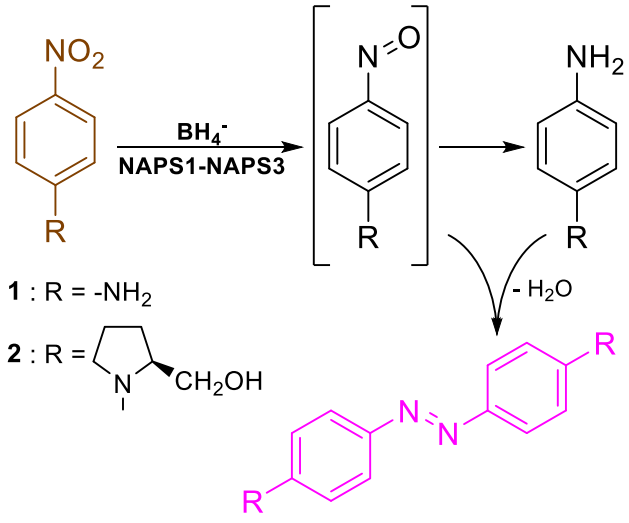

Scheme 2. Reduction of nitroarenes.

Finally, Ag NPs have been reported to catalyze the oxidative coupling of aromatic amines to the relevant azobenzene under air (O_2 is the actual oxidant, Scheme 4).[27] We tested our materials as catalysts for the reaction with aniline **3**, under conditions comparable with literature reports (DMSO, 60 °C, 1 eq. of KOH, 24 h).[27] The observed final yield in the azobenzene **4** varied depending on the catalyst (59% for **NAPS1**, 72% for **NAPS2**, 83% for **NAPS3**, 54% for **NAPS4**). The performance of **NAPS3** is particularly interesting, being comparable with the best results reported;[27] however, attempts to recover and re-use the catalysts were unsatisfactory. In fact, use of **NAPS3** in a second cycle reduced yields to 67%. Rationalizing these results is not straightforward. Based on analytical and porosimetric data, the catalyst efficiency probably depends on a compromise between metal loading and pore size. The poor recyclability might be due to catalyst damage under the mechanical stress of the reaction conditions, preventing quantitative recovery of intact catalyst.

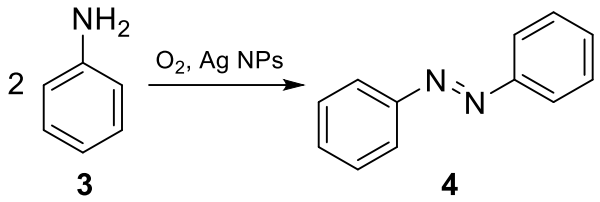

Scheme 3. Oxidative coupling of aniline.

Conclusions

This work describes the preparation of composites constituted by Ag NPs in a polyamine-CDNS matrix, by means of an easy and viable procedure. The polyamine groups of the nanosponge materials are able to capture Ag^+ ions from aqueous solution, and then likely interact with the Ag NPs, which are formed by in situ reduction with $NaBH_4$. The NS structure, indeed, appears to function as a sort of template for the formation of the Ag NPs. The obtained materials show a high metal loading, with substantial maintenance of the chemical structure of the NS architecture. The Ag NPs show a relatively small average diameter, but may undergo significant aggregation depending on the polyamine linker present in the NS. The composites possess remarkable abilities as catalysts of model reactions, i.e. the reduction of *p*-nitroanilines and the oxidative coupling of aniline. Our results positively indicate a synergistic contribution on the reaction course from the interaction between the nanosized metal and the NS. The latter one effectively captures the organic substrate and concentrates it in proximity of the Ag catalyst, affording enhanced activity. This synergism is, in our opinion, a particularly valuable result achieved in the present work. It should be considered that the well-known chemical versatility of the CD scaffold easily allows the synthesis of systems with tailored properties; so, chemically modified NSs with tunable properties can be obtained.[14,28] Thus, the results presented herein constitute an example of how smart composite systems might be designed to supply improved catalytic performance in terms of both reactivity and selectivity. In perspective, this may be useful for setting up large-scale processes with low environmental impact.

Experimental Section

Materials. All the reagents and solvents needed were used as purchased (Aldrich, Fluka) with no further purification. A stock $AgNO_3$ 0.15 M solution was prepared by dissolving 254.8 mg (1.5 mmoles) of $AgNO_3$ in 100 mL of freshly double-distilled water; the solution was kept in the dark and used. within few days. The pristine nanosponges **ANS1**-**ANS4** had been prepared in a previous work. In brief, the *heptakis*-(6-bromo)-(6-deoxy)-β-**CD** was mixed with an equivalent amount of the proper ACD (prepared in turn according to the procedure reported elsewhere,[14] by reacting the same *heptakis*-(6-bromo)-(6-deoxy)-β-**CD** with an excess of the proper polyamine **A1**-**A4**). Then, DMSO (0.4 mL per g of reactant mixture) was added in order to obtain a thick paste, which was kept still for 48 h at 60 °C. The resulting amorphous solid was then mechanically disgregated and washed several times with water, methanol and diethyl ether. Finally, it was crushed in a mortar, passed through a 150-μm sieve, and dried in vacuo over P_2O_5 at 50 °C overnight. The isolated material (as partial hydrobromides) are quantitatively characterized by means of a potentiometric titration, which allowed in particular to determine the average number of polyamine linkers and formally retained HBr molecules per CD unit (see the reference work for details). Analytical data relevant to materials **ANS1**-**ANS4** are summarized in the Supporting Information (Table S1). The non-commercial *N*-(*p*-nitrophenyl)-L-prolinol was prepared by an aromatic nucleophilic displacement reaction between *p*-nitro-fluorobenzene and L-prolinol.[6d]

Instrumentation. UV-vis spectra were recorded on a Beckmann Coulter DU 800 spectrophotometer, equipped with a Peltier thermostatic apparatus. FTIR spectra on powders were acquired on a Bruker VERTEX70 instrumentation. Solid-state NMR spectra were recorded on a Bruker Avance III (600 MHz) spectrometer equipped with a 15 KHz rotating MAS probe. Thermogravimetric analyses were performed on a TA Instruments TGA Q5000 apparatus; samples were heated under a continuous nitrogen stream (25 mL/min) up to 850 °C at a 25 °C/min heating rate. Scanning electron microscopy analyses were carried out using a field-emission Zeiss SUPRA® 40VP scanning electron microscope. A 2 μL drop of each sample was spread on freshly cleaved mica sheet, dried at 37°C, and sputter-coated with a gold-platinum alloy for 15 s at 10 mA (SC7620 Sputter coater). Micrographs were acquired using the InLens (secondary electron) mode with an accelerating voltage of 10 kV. High resolution TEM micrographs were acquired on a JEOL JEM-2100 electron microscope operating at 200 kV acceleration voltage; a drop of a suspension of each material in isopropyl alcohol was placed on a 3 mm Cu grid “lacey carbon”, and the solvent was allowed to evaporate completely before acquiring the micrographs.

Synthesis of composites NAPS1-NAPS4. The synthesis occurs in two steps. First, four precursor materials **P1**-**P4** were prepared as follows: 1 meq of each pristine NS (i.e. 336.4 mg of **ANS1**, 296.4 mg of **ANS2**, 212.8 mg of **ANS3**, 196.4 mg of **ANS4**) was mixed to 10 mL of stock $AgNO_3$ 1.5 mM solution, and the suspension (covered in tinfoil to avoid exposure to light) was mechanically shaken for 90 min. The system was then centrifuged and the supernatant liquor was eliminated. The solid residue was washed in sequence with 5 mL of water, 5 mL of methanol and 5 mL of diethyl ether, placed in a dark vial, dried in vacuo over P_2O_5 at 30 °C overnight, and stored in the same apparatus before use. Yields:

499.4 mg for **P1**; 524.0 mg for **P2**; 343.6 mg for **P3**; 293.2 mg for **P4**. In the second step, the final composites **NAPS1**-**NAPS4** were prepared as follows: each precursor material coming from the previous step was suspended in 7 mL of water at r.t. under magnetic stirring. Then, 3 mL of a freshly prepared aqueous $NaBH_4$ 0.5 M were added dropwise to the suspension, and the system was kept under magnetic stirring overnight. The black solid product was collected by centrifugation and washed repeatedly several times with water (5 mL), until the washing liquors were colorless. The product was then subjected to one further washing with methanol (5 mL) and one with diethyl ether (5 mL); finally, it was dried in vacuo over P_2O_5 at 30 °C overnight and stored in the same apparatus. Yields: 414.1 mg for **NAPS1**; 381.6 mg for **NAPS2**; 281.8 mg for **NAPS3**; 259.0 mg for **NAPS4**

Analysis of TGA data. In order to calculate the $AgNO_3$ loading for materials **P1**-**P4** it should preliminarily considered that the residual % at 850 °C of the pure salt (R_S) is 62.7 %. Then, indicating as R_{NS} and R_P the residual % of the pristine polyamine-**CDNS** and the relevant **P**-type material (corrected for the unavoidable loss of residual water before 150 °C, which is clearly apparent from TGA curves), and as χ_{AgNO3} the weight fraction of $AgNO_3$, it can be assumed that:

$$R_P = R_S \cdot \chi_{AgNO3} + R_{NS} \cdot (1- \chi_{AgNO3})$$

Therefore, χ_{AgNO3} can be easily calculated by trivial algebraic passages. Similarly, indicating as R_{NAPS} the corrected residual % of the the relevant **NAPS**-type material, and as χ_{Ag} the weight fraction of Ag (which of course suffers no weight loss on heating), we have:

$$R_{NAPS} = 100 \cdot \chi_{Ag} + R_{NS} \cdot (1- \chi_{Ag})$$

from which χ_{Ag} can be easily obtained. Finally Ag/N mole ratios can be deduced by trivial algebraic passages, using the analytical data reported on Table S1 of the Supporting Information.

Reduction of nitroarenes. In a screw-cap vial, 60 μL of a stock 5 mM solution in methanol of either *p*-nitroaniline (**1**) or *N*-(*p*-nitrophenyl)-L-prolinol (**2**) were added to 2.69 mL of water. The vial was warmed and kept at 40 °C; then, under magnetic stirring, 250 μL of a freshly prepared 60 mM aqueous solution of $NaBH_4$ were introduced. The time needed to achieve the discoloration of the initially vivid yellow solution was recorded; then an aliquot of the solution was rapidly pipetted, and its UV-vis spectrum was recorded to verify the complete disappearance of the peculiar absorption band of the substrate, centered at λ_{max} 378 nm (ε = 18700) for **1** or 420 nm (ε = 22700) for **2**. For the flow reaction, a home-made reactor was built inserting a tiny glass tube (4 mm diameter) into a thermostatic jacket made in copper sheet, connected with a thermostatic bath (40 °C); 100 mg of material **NAPS2** were introduced into the glass tube. Then, the solution of the reactants prepared as described above was passed through the material at a flow rate of 1.2 mL/min (in the case of **1**) or 0.6 mL/ min (in the case of **2**), and the UV-vis spectrum of the resulting eluate was recorded to verify the conversion of the substrate.

Oxidative coupling of aniline. Freshly distilled aniline (90 μL, 93 mg, 1.0 mmoles) and KOH (56.0 mg, 1.0 mmoles) were dissolved in 4 mL of DMSO; then the catalyst (10 mg) was added, and the mixture was kept at 60 °C under magnetic stirring for 24 h. Then, the reaction mixture was centrifuged, and the supernatant liquor is poured dropwise into 30 mL of water. The aqueous phase is extracted thrice with ethyl acetate (20 mL each), whereas the residue solid catalyst is washed with few mL of methanol. The combined organic extracts were dried (Na_2SO_4) and distilled in vacuo to afford a crude mixture, which was ultimately chromatographed to recover the pure azobenzene product.

Acknowledgements

Solid-state NMR spectra were acquired at CHAB-ATeN Center, Università di Palermo; TEM micrographs were acquired at CGA-ATeN Center Università di Palermo, funded by *P.O.R. Sicilia 2000-2006, Misura 3.15 Quota Regionale*; Dr. G. Nasillo is gratefully acknowledged. Prof. D. Chillura Martino (Dept. STEBICEF, University of Palermo) is sincerely acknowledged for very useful discussion and advices.

Keywords: Cyclodextrins • Nanosponges • Nanoparticles • Silver • Catalysis

[1] a) J. S. Bradley, E. W. Hill, C. Klein, B. Chaudret, A. Duteil, *Chem. Mater.* **1993**, *5*, 254-256; b) D. S. Shephard, T. Maschmeyer, G. Sankar, J. M. Thomas, D. Ozkaya, B. F. G. Johnson, R. Raja, R. D. Oldroyd, R. G. Bell, *Chem. Eur. J.* **1998**, *4*, 1214-1224; c) K. E. K. Torigoe, *Langmuir* **1993**, *9*, 1664–1667; d) L. H. Tu W., *Chem. Mater.* **2000**, *12*, 564–567; e) M. Paskevicius, J. Webb, M. P. Pitt, T. P. Blach, B. C. Hauback, E. M. Gray, C. E. Buckley, *J. Alloys Compd.* **2009**, *481*, 595-599.

[2] a) V. Polshettiwar, R. S. Varma, *Green Chemistry* **2010**, *12*, 743-754; b) S. B. Kalidindi, B. R. Jagirdar, *Chemsuschem* **2012**, *5*, 65-75; c) B. H. Lipshutz, N. A. Isley, J. C. Fennewald, E. D. Slack, *Angewandte Chemie-International Edition* **2013**, *52*, 10952-10958.

[3] H.-L. Jiang, Q. Xu, *J. Mater. Chem.* **2011**, *21*, 13705-13725.

[4] a) R. Cavalli, F. Trotta, W. Tumiatti, *J. Incl. Phenom. Macrocycl. Chem.* **2006**, *56*, 209-213; b) S. S, A. S, K. Krishnamoorthy, M. Rajappan, *J Pharm Pharm Sci* **2012**, *15*, 103-111; c) F. Trotta, in *Cyclodextrins in Pharmaceutics, Cosmetics, and Biomedicine*, John Wiley & Sons, Inc., **2011**, pp. 323-342.

[5] M. V. Rekharsky, Y. Inoue, *Chem. Rev.* **1998**, *98*, 1875-1918.

[6] a) L. Liu, Q.-X. Guo, *J. Incl. Phenom. Macrocycl. Chem.* **2002**, *42*, 1-14; b) M. Rekharsky, Y. Inoue, *J. Am. Chem. Soc.* **2000**, *122*, 4418-4435; c) P. Lo Meo, F. D'Anna, S. Riela, M. Gruttadauria, R. Noto, *Tetrahedron Lett.* **2006**, *47*, 9099-9102; d) P. Lo Meo, F. D'Anna, S. Riela, M. Gruttadauria, R. Noto, *Tetrahedron* **2007**, *63*, 9163-9171; e) P. Lo Meo, F. D'Anna, S. Riela, M. Gruttadauria, R. Noto, *Tetrahedron* **2009**, *65*, 2037-2042; f) P. Lo Meo, F. D'Anna, M. Gruttadauria, S. Riela, R. Noto, *Tetrahedron* **2004**, *60*, 9099-9111.

[7] A. R. Khan, P. Forgo, K. J. Stine, V. T. D'Souza, *Chem. Rev.* **1998**, *98*, 1977-1996.

[8] a) P. Lo Meo, G. Lazzara, L. Liotta, S. Riela, R. Noto, *Polym. Chem.* **2014**, *5*, 4499-4510; b) Y.-Z. Du, J.-G. Xu, L. Wang, H. Yuan, F.-Q. Hu, *Eur. Polym. J.* **2009**, *45*, 1397-1402; c) J. Huot, D. B. Ravnsbæk, J. Zhang, F. Cuevas, M. Latroche, T. R. Jensen, *Prog. Mater Sci.* **2013**, *58*, 30-75.

[9] H. Li, B. Meng, S.-H. Chai, H. Liu, S. Dai, *Chemical Science* **2016**, *7*, 905-909.

[10] D. A. Vasconcelos, T. Kubota, D. C. Santos, M. V. G. Araujo, Z. Teixeira, I. F. Gimenez, *Carbohydr. Polym.* **2016**, *136*, 54-62.

[11] a) S. Sadjadi, M. M. Heravi, M. Malmir, *Carbohydr. Polym.* **2018**, *186*, 25-34; b) S. Sadjadi, M. M. Heravi, M. Raja, *Carbohydr. Polym.* **2018**, *185*, 48-55.

[12] R. Martin-Trasanco, R. Cao, H. E. Esparza-Ponce, M. E. Montero-Cabrera, R. Arratia-Pérez, *Carbohydr. Polym.* **2017**, *175*, 530-537.

[13] a) R. Herbois, S. Noel, B. Leger, S. Tilloy, S. Menuel, A. Addad, B. Martel, A. Ponchel, E. Monflier, *Green Chemistry* **2015**, *17*, 2444-2454; b) S. Noel, D. Bourbiaux, N. Tabary, A. Ponchel, B. Martel, E. Monflier, B. Leger, *Catal. Sci. Technol.* **2017**, *7*, 5982-5992; c) S. Noel, B. Leger, A. Ponchel, F. Hapiot, E. Monflier, in *Iconbm: International Conference*

on Biomass, Pts 1 and 2, Vol. 37 (Eds.: E. Ranzi, K. KohseHoinghaus), Aidic Servizi Srl, Milano, **2014**, pp. 337-342.

[14] M. Russo, M. L. Saladino, D. Chillura Martino, P. Lo Meo, R. Noto, *RSC Adv.* **2016**, *6*, 49941-49953.

[15] a) M. Russo, D. La Corte, A. Pisciotta, S. Riela, R. Alduina, P. Lo Meo, *Beilstein J. Org. Chem.* **2017**, *13*, 2751-2763; b) P. Lo Meo, F. D'Anna, M. Gruttadauria, S. Riela, R. Noto, *Carbohydr. Res.* **2012**, *347*, 32-39.

[16] M. Russo, F. Armetta, S. Riela, D. Chillura Martino, P. Lo Meo, R. Noto, *J. Mol. Catal. A: Chem.* **2015**, *408*, 250-261.

[17] a) M. Russo, A. Meli, A. Sutera, G. Gallo, D. Chillura Martino, P. Lo Meo, R. Noto, *RSC Adv.* **2016**, *6*, 40090-40099; b) M. Russo, D. C. Martino, E. Caponetti, P. Lo Meo, *ChemistrySelect* **2018**, *3*, 3048-3055.

[18] X. Y. Dong, Z. W. Gao, K. F. Yang, W. Q. Zhang, L. W. Xu, *Catal. Sci. Technol.* **2015**, *5*, 2554-2574.

[19] K.-S. Lee, M. A. El-Sayed, *J. Phys. Chem. B* **2006**, *110*, 19220-19225.

[20] S. Eckhardt, P. S. Brunetto, J. Gagnon, M. Priebe, B. Giese, K. M. Fromm, *Chem. Rev.* **2013**, *113*, 4708-4754.

[21] J. J. Blaker, A. R. Boccaccini, S. N. Nazhat, *J. Biomater. Appl.* **2005**, *20*, 81-98.

[22] a) J. Caloca, L. Z. Flores-Lopez, H. Espinoza-Gomez, E. L. Sotelo-Barrera, A. Nunez-Rivera, R. D. Cadena-Nava, *Cellulose* **2017**, *24*, 4997-5012; b) M. I. Martinez-Espinoza, M. Maccagno, S. Thea, M. Alloisio, *Appl. Surf. Sci.* **2018**, *427*, 724-732; c) S. M. Osman, S. N. Khattab, E. A. Aly, E. Kenawy, A. El-Faham, *Journal of Polymer Research* **2017**, *24*.

[23] a) M. T. Bilkan, Ş. Yurdakul, Z. Demircioğlu, O. Büyükgüngör, *J. Organomet. Chem.* **2016**, *805*, 108-116; b) B. Morzyk-Ociepa, D. Michalska, *Spectrochimica Acta Part A: Molecular and Biomolecular Spectroscopy* **1999**, *55*, 2671-2676.

[24] a) H. Mustroph, *Dyes and Pigments* **1991**, *15*, 129-137; b) H. Mustroph, *Dyes and Pigments* **1991**, *16*, 223-230.

[25] a) D. M. Dotzauer, S. Bhattacharjee, Y. Wen, M. L. Bruening, *Langmuir* **2009**, *25*, 1865-1871; b) M. V. Parmekar, A. V. Salker, *RSC Adv.* **2016**, *6*, 108458-108467.

[26] a) P. Lo Meo, F. D'Anna, S. Riela, M. Gruttadauria, R. Noto, *Tetrahedron* **2002**, *58*, 6039-6045; b) P. Lo Meo, F. D'Anna, M. Gruttadauria, S. Riela, R. Noto, *Tetrahedron* **2009**, *65*, 10413-10417.

[27] H. R. S. Cai, X. Yu, X. Liu, D. Wang, W. He, Y. Li, *ACS Catal.* **2013**, *3*, 478–486.

[28] V. Cinà, M. Russo, G. Lazzara, D. Chillura Martino, P. Lo Meo, *Carbohydr. Polym.* **2017**, *157*, 1393-1403.

Entry for the Table of Contents

Insert graphic for Table of Contents here.

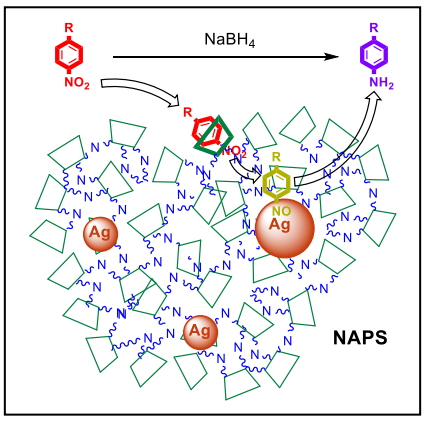

Synergism at the nanoscale: exploiting the inclusion abilities of nanosponges results in a remarkable improvement in the catalytic abilities of new silver nanoparticle composites towards typical probe reactions such as nitroarene reduction or aniline oxidative coupling.